Investigation of the impact of hydrostatic stress on mechanical, optical, and structural properties of cubic $SrSnO_3$

S. M. JUNAID ZAIDI[1], WASEEM AMIN[2], ALI ABDULLAH[3], MUHAMMAD UMER FAROOQ[4], NAEEM ULLAH[5], M. SANA ULLAH SAHAR[6], M. IJAZ KHAN[4,*]
[1]*Department of Physics and Mathematics, Faculty of Sciences, Superior University, Lahore 54000, Pakistan*
[2]*Institute of Metallurgy and Materials Engineering, University of the Punjab, 54801, Lahore, Pakistan*
[3]*Department of Physics, University of Management and Technology, Sialkot Campus, Sialkot,51310, Pakistan*
[4]*Institute of Mechanical and Manufacturing Engineering, Khwaja Fareed UEIT, Rahim Yar Khan, 64200, Pakistan*
[5]*Department of Mechanical Engineering Technology, Punjab Tianjin University of Technology, Lahore 54770, Pakistan*
[6]*Department of Mechanical Engineering, University of Sargodha, Sargodha - 40100, Pakistan*

This study comprehensively explored the various characteristics of $SrSnO_3$ when subjected to a mechanical load with the help of an ultrasoft pseudopotential (USP) and the generalized gradient approximation (GGA). The crystal lattice remains cubic, but a significant decrease of 11% in the lattice parameters and a 29% decrease in the lattice volume are observed. Moreover, no phase transformation is observed. The mechanical load not only affects the electronic structure but also impacts the way the material responds to optical load, including properties such as reflectivity, refractive index, absorption, energy loss function, and complex dielectric function. The increase in the absorption peak and the shift of these peaks to higher energies confirm the occurrence of a blue shift, which renders this material an attractive aspirant for optoelectronic applications. Furthermore, the material is inflexible, rigid, and mechanically stable and shows high resistance to shear deformation, which is confirmed by computing various mechanical parameters, including the Young, shear, and bulk moduli. Moreover, the Cauchy pressure, Pugh/Frantsevich ratio, and Poisson's ratio revealed the metallic bond structure, ductile behavior, and high-pressure strength of the material. The electronic band structure (BS) of $SrSnO_3$ changes from a narrow band (0.135 eV) to a wide band (4.682 eV). The total, partial, and elemental partial density of states (TDOS/PDOS) were recorded for the analysis of the electronic band structure. It is the best material to be utilized as an ultraviolet filter since its absorption spectra are present in the UV range. Moreover, its absorption, high conductivity, refractive index, and reflectivity make it an exceptional component in optoelectronic devices.

(Received March 13, 2025; accepted February 4, 2026)

Keywords: Perovskite, Band gap, Elastic constants, Mechanical properties, Optical properties

1. Introduction

Perovskites have received much attention from researchers in the modern scientific era and have been rigorously studied owing to their attractive set of properties, including ferroelectricity, piezoelectric properties, high-temperature superconductivity (HTS), ionic and electronic conductivity, catalytic properties, and thermal stability. Perovskites have numerous applications as substrates or catalytic electrodes in fuel cells or as sensors in optoelectronic and spintronic devices [1]. ABO_3 is defined by the general chemical formula of perovskite oxides, where A and B are two distinct cations. Perovskite oxides have a flawless cubic lattice, but most of them are significantly deformed and lack symmetry [2]. Structural analysis of the strontium sulfonate ($SrSnO_3$) lattice showed that it fits into the pm-3m group phase. Strontium inhabits the (0, 0, 0) location, Tin/Sn occupies the (0.5, 0.5, 0.5) location, and oxygen holds the (0.5, 0.5, 0), (0.5, 0, 0.5) and (0, 0.5, 0.5) locations in the crystal lattice [3]. Strontium stannates ($SrSnO_3$) have many potential technological applications. It has been reported to be a favorable photocatalyst. Water can be split into hydrogen and oxygen by its valence and conduction band edge positions. The major limitation of $SrSnO_3$ is its large band gap of 4.1 eV, indicating that it can absorb waves lying only in the ultraviolet region [1,3,4].

$SrSnO_3$ is a perovskite and alkaline earth hydrolysate. Such stannates have received significant attention in the recent past for their use in various applications, e.g., in the energy and environmental sectors. $SrSnO_3$ has found several applications, e.g., in high-temperature nitrogen oxide sensors, high-temperature humidity sensors, and lithium-ion batteries. Moreover, $SrSnO_3$ has also been used as a photocatalyst material owing to its good photocatalytic action, which can be related to the structure of the $SrSnO_3$ lattice [2,5-8]. Bezerra *et al*. [3] simulated the electronic and structural properties of $SrSnO_3$ by analyzing the band gap and performing XRD. They implemented the B3LYP exchange-correlation function with the CRYSTAL14 code. They found that a = b = c = 4.080 Å, volume = 67.917 $Å^{3,}$ and band gap = 4.18 eV. Arya *et al*. [4] simulated the cubic

structure of $SrSnO_3$ to determine its structural, optical, electronic, and thermoelectric properties. They employed the modified Becke-Johnson potential proposed by Tran and Blaha (TB-mBJ) for band gap calculations. All the calculations were performed in the WEIN2K software. The lattice parameters were found to be a = b = c = 4.12 Å. They found negative values of the dielectric constant at 24-28 eV, which shows that in this region, the material reflects. Bezerra *et al*. [9] examined the both structural and electronic characteristics of strontium stannate in cubic form. The results showed the cubic symmetry of the material. The lattice constant determined from their results is 4.080 Å, and the corresponding volume is 67.917 $Å^3$.

In this work, we present in detail the consequence of induced stress (0–100 GPa) on the optical, structural, elastic, and mechanical properties of cubical $SrSnO_3$. We applied exchange-correlation of Generalized-Gradient Approximation-Perdew Burke Ernzerhof (GGA-PBE). To apply this approximation a Cambridge Serial Total Energy Package (CASTEP) code was employed, which has never been reported before in the literature.

2. Simulation setup

In this study, the Material Studio setup is used for performing calculations. The CASTEP code is considered by operating the moralities of density functional theory (DFT) [10]. For the electron transference GGA approximation was used which is established by Perdew-Burke-Ernzerhof (PBE) [11,12]. The computational GGA approximation is applied to cubic $SrSnO_3$, which has a space group pm-3m, under the influence of different applied stress values of 0, 20, 40, 60, 80, and 100 GPa for a 2x2x2 supercell [13], as shown in Fig. 1(a). A Monkhorst-Pack grid (MPG) of 2x2x2 fine k-points was used for Brillouin zone integration [14]. The energy cutoff for this simulation was set to 340 eV for the description of electron-ion interactions by the ultrasoft pseudopotential [13,15]. In the whole simulation, the band energy tolerance was set to 1×10^5 eV [16].

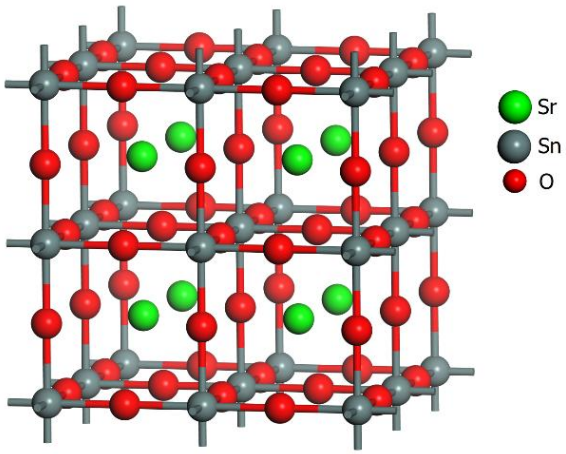

Fig. 1. Supercell of $SrSnO_3$ (colour online)

It is evident from Fig. 1(b) that there is an exponential decrease in the lattice parameters and lattice volume values gradually from 4.17632–3.73256 Å and 72.8419–52.0020 $Å^3$, respectively, with a gradual increase in stress up to 100 GPa. The calculations are based on the Kohn–Sham equations [11,12,17].

3. Results

3.1. Geometry optimization

The crystal lattice of $SrSnO_3$ and its mechanical properties are also influenced by the application of mechanical loads. Fig. 3 shows the gradual decrease in the lattice parameters and the lattice volume with increasing applied stress from 0 to 100 GPa. An increase in the stress on $SrSnO_3$ reduces its lattice parameter from 4.17632 Å to 3.73256 Å at 100 GPa, i.e., a decrease of 11% is observed, whereas a decrease of 29% is observed in the lattice volume.

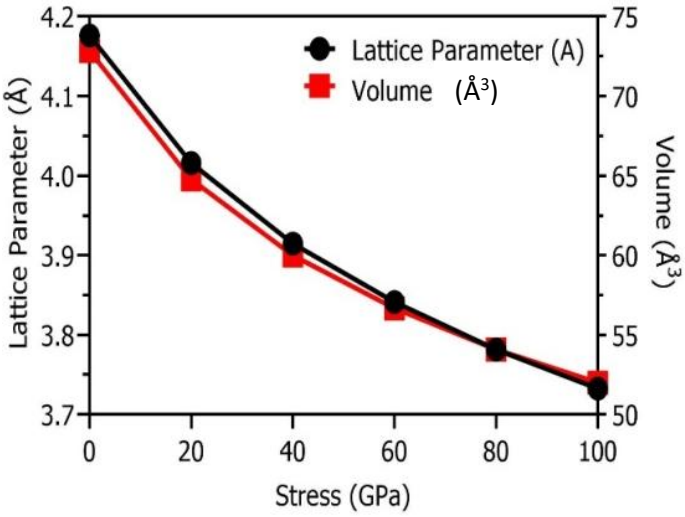

Fig. 2. Lattice parameter and volume variation with stress (colour online)

Table 1. Comparison of lattice parameters (Å) and unit cell volumes ($Å^3$) for cubic $SrSnO_3$

$SrSnO_3$	Lattice Parameters a=b=c	Unit Cell Volume	Reference
This Work	4.176	72.8419	-
Theoretical	4.080 4.080 4.111	67.917 - 69.477	[3] [4] [18]
Experimental	4.040 4.032	65.939 65.548	[19] [20][21]

3.2. Electronic properties

3.2.1. Density of states

A basic method for thoroughly examining the various facets of the band structure is the application of partial and

total densities of states (PDOS and TDOS). In quantum dynamics, the Fermi Golden Rule gives the probability that a disturbance will cause a quantum system to change from an initial state to a final state, a theoretical background for determining optical absorption rates. Moreover, electrical conductivity is an effective means of measuring the number of mobile states present in a substance through the utilization of these sophisticated techniques, and scientists can acquire a deep understanding of the intricate details present in the band structure, elucidating crucial characteristics linked to electron dynamics, absorption occurrences, and general charge carrier mobility. The partial densities of states (PDOS) of Sr, Sn, and O are shown in Figs. 3-5. The foremost contribution for the creation of the higher portion of the valence band in $SrSnO_3$ at 0 GPa is owing to the *p* orbitals of O, while the bottom portion valence band is formed due to the *p* orbitals of the Sr and *s*-orbital of O. The contributions of Sr "d" and Sn's "s" orbitals resulted in the development of the conduction band.

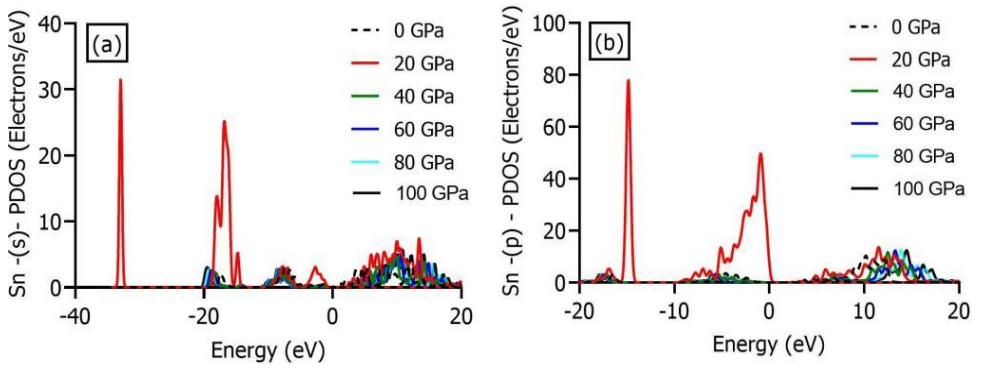

Fig. 3. Partial density of states (PDOS) of tin (Sn) under stresses ranging from 0 to 100 GPa (a) s-orbital contribution, (b) p-orbital contribution (colour online)

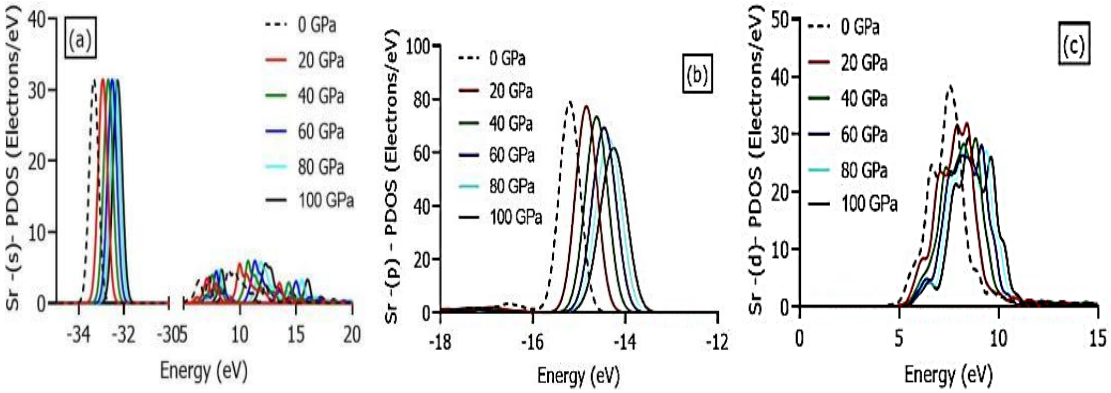

Fig. 4. Partial density of states (PDOS) of strontium (Sr) under stresses ranging from 0 to 100 GPa (a) s-orbital, (b) p-orbital and (c) d-orbital contribution (colour online)

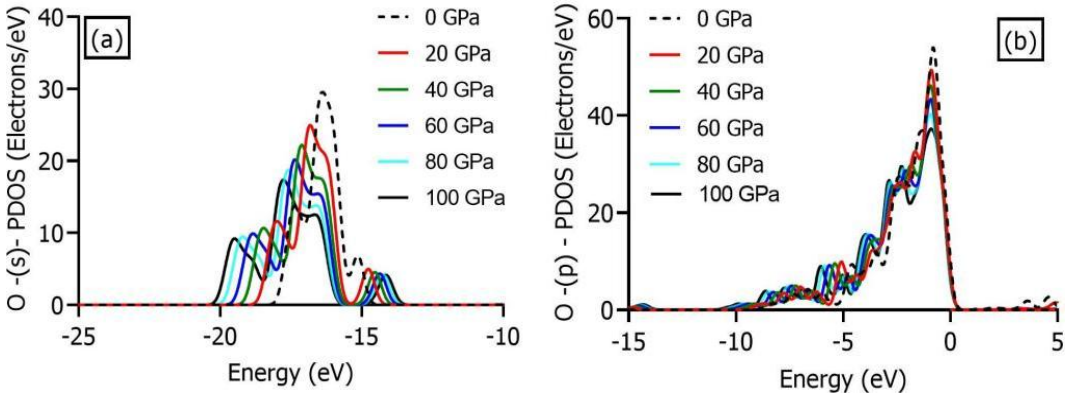

Fig. 5. Partial density of states (PDOS) of oxygen (O) under stresses ranging from 0 to 100 GPa (a) s-orbital and (b) p-orbital contribution (colour online)

Fig. 6 demonstrates that the band expansion phenomena are indicated by the TDOS as a function of energy, which highlights the important influence of induced stress (0–100 GPa) on the electronic characteristics and results in observable variations in the TDOS peak intensities.

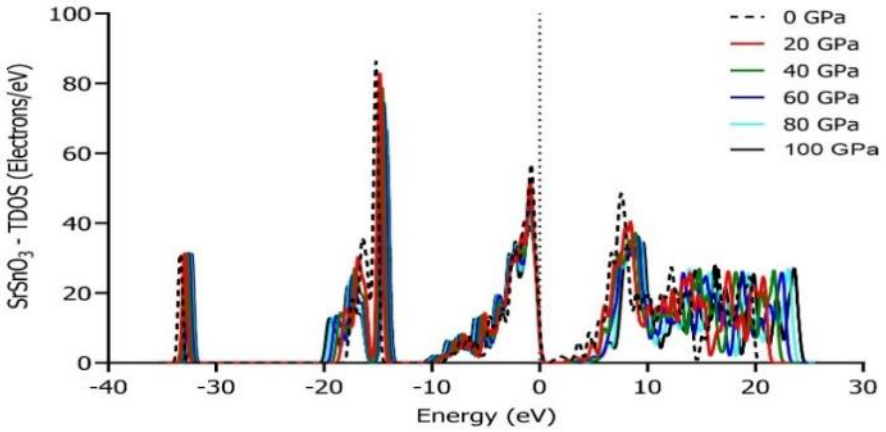

Fig. 5. TDOS of SrSnO3 under stresses of 0 GPa, 20 GPa, 40 GPa, 60 GPa, 80 GPa, and 100 GPa (colour online)

The gap is widened by increased stress because it shortens the Sn–O bond length, which pushes Sn-5s conduction band states upward and reduces the contribution of O-2p levels close to the valence band maximum. In the updated version, we have provided an explanation.

3.3. Elastic and mechanical properties

As the bond length changes, the response to external loads on the crystal also changes. Fig. 7 shows the variation in the stiffness tensor components [22,23]. As stress rises from 0 to 100 GPa, a drastic increase of more than 4 times is observed in the magnitude of C_{11}, and an increase of more than 5 times is observed in C_{12}, whereas C_{44} increases by only 1.4 times. These results indicate that the material becomes stiffer in principle crystallographic directions, the change in any specific direction also changes in the perpendicular direction, and $SrSnO_3$ has greater shear resistance. Furthermore, these results indicate the nonlinear behavior of the material with the application of external stress. Stiffer materials have numerous applications in aerospace, automotive, and structural engineering.

These stiffness tensor components contribute to the estimation of different elastic moduli of the material; hence, Fig. 8a shows that the bulk modulus [24,25] increased from 124.4 to 561.9, the shear modulus [26,27] from 87.9 to 193.3, and Young's Modulus [28,29] from 213.5 to 520.3. These results indicate that the $SrSnO_3$ material becomes less compressible with the application of stress and that the material resists shear deformation with the application of stress, resulting in a stiffer response to compressive stress.

Fig. 8b shows that the Frantsevich ratio [30] decreases from 0.707 to 0.34, and the anisotropic factor [31,32] decreases from 0.72 to 0.25, and Poisson's ratio [33,34] increases from 0.21 to 0.34. Fig. 8c shows that the Pugh ratio [35] increases from 1.4 to 2.9, and the Cauchy pressure [24] increases from –0.24 to 172.47. These results show that some quantities are strongly influenced by the applied stress when the applied stress increases from 20 GPa to 40 GPa.

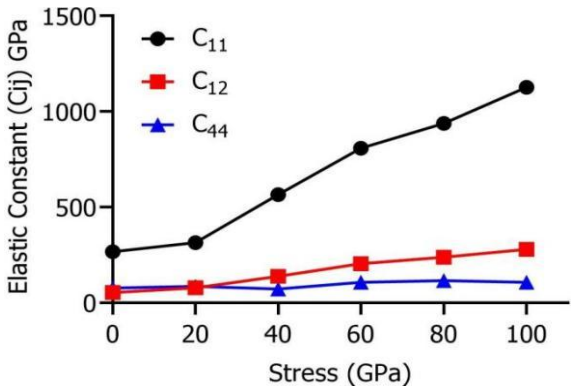

Fig. 6. Variation in the elastic constant with stress (colour online)

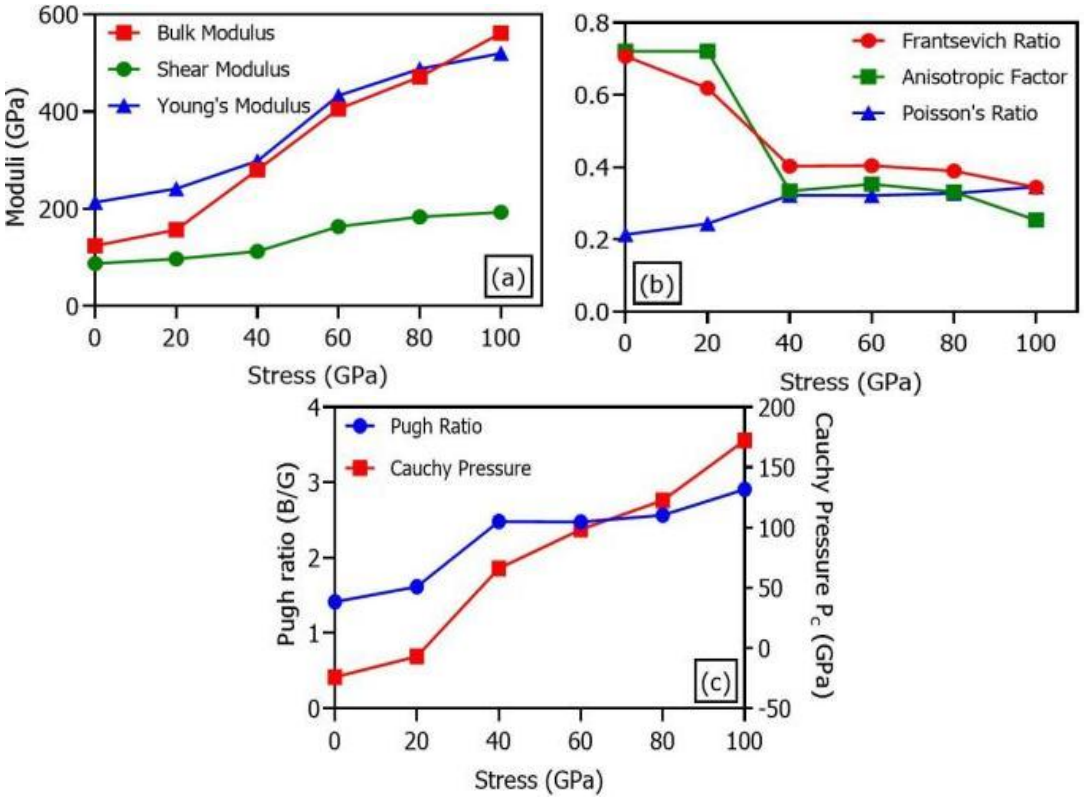

Fig. 7. (a) Bulk modulus (B), shear modulus (G), Young's modulus (E), (b) Frantsevich ratio (G/B), anisotropic factor (A), Poisson's ratio, (c) Pugh ratio (B/G) and Cauchy pressure (CP) as a function of stress applied to the SrSnO3 crystal (colour online)

3.4. Optical properties

Strontium Stannates are attractive candidates for applications in electro-optic devices; therefore, the influence of stress on the optical properties of $SrSnO_3$ lattices has been evaluated. Optical characteristics, such as refractive indices [36], absorption coefficient [37], reflectivity [38], dielectric function [29], and the energy loss function [39] explain the light-matter interaction. These characteristics of cubic $SrSnO_3$ under the influence of applied stress (0, 20, 40, 60, 80, 100 GPa) were computed and are shown in Fig. 9(a–f). These optical properties are coupled with one other and are frequency-dependent. All other attributes can be determined if the function of complex dielectric is computed using Maxwell's equations.

First, the absorption spectrum is evaluated, as shown in Fig. 9a. This reveals that the absorption of $SrSnO_3$ is significant in the ultraviolet region of the electromagnetic spectrum. Here, it is important to mention that the threshold absorption point seems at around 9.0 eV. The degree of absorption rises in direct proportion to energy. It can also be observed that the absorption edge sets at 9.0 eV in the stress-free lattice, and when stress is applied, the absorption edge starts to shift to higher energies. As a result, the absorption spectrum blue shifts, sharpening the peaks and shifting them to the right. The maximum peak shift can be observed at 38.50 eV for $SrSnO_3$. Our projected density of states (PDOS) analysis shows that the Valence Band Maximum VBM is primarily O-2p dominated, while the CBM has significant Sn-5s character. Under hydrostatic stress, there is less overlap between the Sn-5s and O-2p orbitals, which lowers hybridization and raises the Conduction Band Minimum CBM to higher energies. This directly leads to the blue shift in optical absorption. A comprehensive orbital-level discussion will be held, complete with PDOS charts.

The maximal absorption is described by explaining transitions in various states of tin and oxygen. The absorption of SrSnO3 agrees with earlier research findings. The results show that the material will absorb high-energy electromagnetic UV waves when stress is applied. Furthermore, $SrSnO_3$ under high stress shows enhanced absorption of electromagnetic radiation. Similarly, the conductivity is also shifted and increased by applying stress to $SrSnO_3$, as shown in Fig. 9b. Enhanced optical conductivity or better electron-photon interactions are beneficial for sensors, photovoltaics, and optoelectronics devices.

The dielectric function of the material is also analyzed through simulation results. Its real component is shown in Fig. 9c. It provides an estimate of the polarization, whereas the imaginary component is an estimation of the energy wasted in the system, and it also helps in understanding the absorption pattern. The static dielectric for 0 GPa is $\epsilon_o = 12.07$, which is a moderate value, so this material can be considered a good dielectric material. This means that the material has moderate dielectric, energy storage, and polarization properties. The material has good capability for energy storage and has applicability in capacitors,

insulating layers, and dielectric resonators. Another important parameter is the energy loss function, as shown in Fig. 9d, which indicates higher energy dissipation, modification of the carrier density of states, and alteration of plasmon resonances. The properties of $SrSnO_3$ at the microscale and macroscale rely on the fast electrons that traverse the lattice. Energy loss occurs during this process and can be estimated with the help of the electron energy loss function. An important peak in the energy loss function spectrum is the plasmon peak. These peaks and other irregular peaks are interdependent.

The reflectivity of $SrSnO_3$ was analyzed, as shown in Fig. 9e. The foremost peak can be observed at approximately 30 eV. The interaction between the d state of strontium and the p state of oxygen in the valance and conduction bands, respectively, is responsible for this appearance in the spectrum. There are some reflectance maxima at 0 GPa. Nonetheless, the reflectivity rises at an energy of about 30 eV as stress rises to 100.0 GPa. Low-energy areas of the energy spectrum, such as the visible, infrared, and ultraviolet regions, are where SrSnO3 is transparent. At approximately 30.0 eV, the reflectivity increases to 65%.

Additionally, examined is the refractive index, which is correlated with the lower absorption energy and has its maximum value at zero photon energy. The magnitude of the refractive index decreases inversely with the absorption, which can be observed in Fig. 9f. The absorption spectrum measures how much light is absorbed by $SrSnO_3$. The results of the refractive index are shown in Fig. 9f. The extreme value of the refractive index obtained is 2.7 at an energy of approximately 8.0 eV.

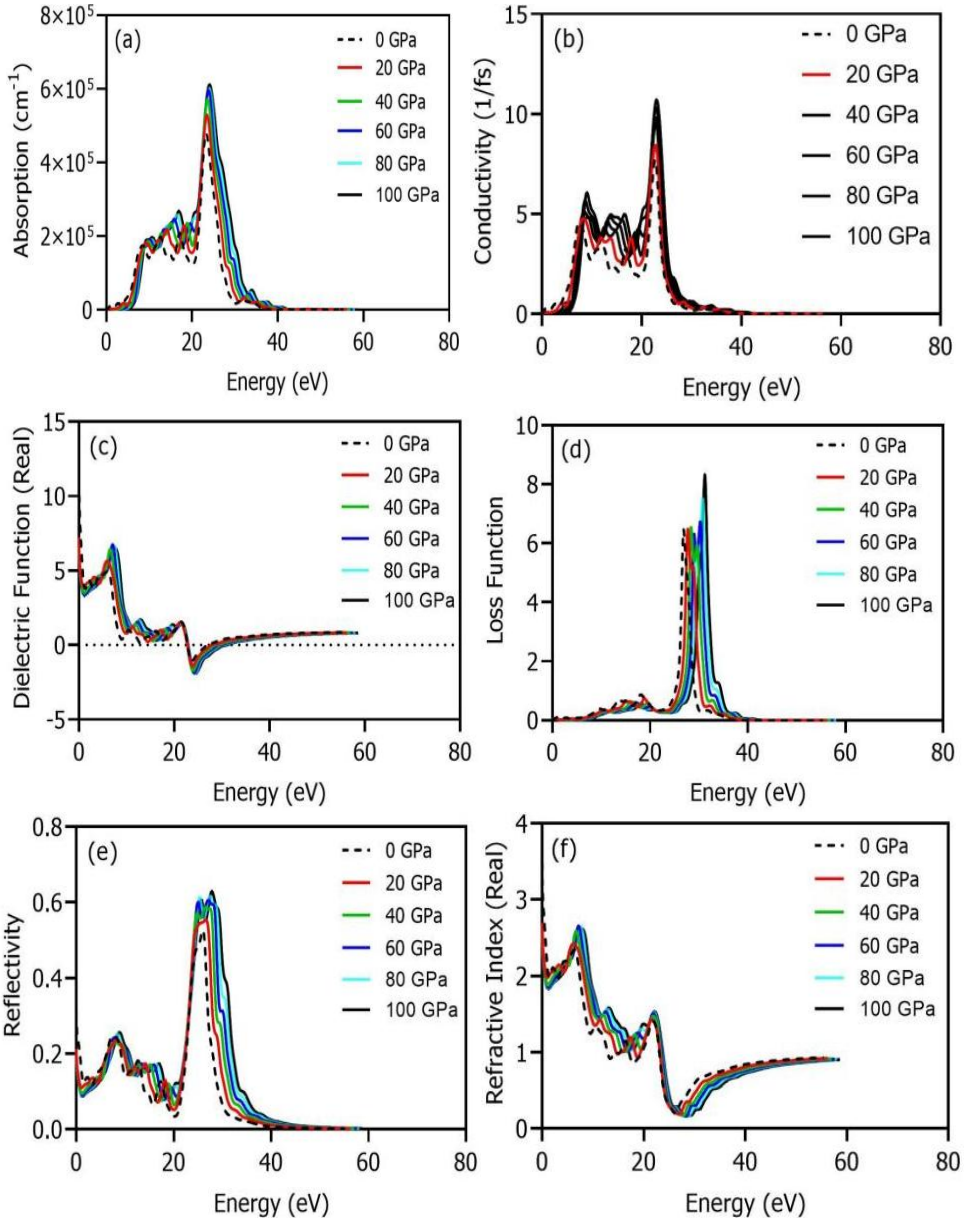

Fig. 8. Optical characteristics of $SrSnO_3$: (a) the absorption spectrum, (b) the conductivity, (c) the real part of the dielectric function, (d) the energy loss function, (d) the reflectivity, (h) the real part of the refractive index, and (i) the imaginary part (colour online)

3.5. X-ray diffraction

An X-ray diffraction simulation was performed for cubic $SrSnO_{3, as}$ shown in Fig. 10, which is consistent with the standard JCPD data card no. 77–1798. When the stress is increased, the intensity peaks are shifted toward the right side or toward a higher angle, which is an indication of internal compressive stress. The maximum diffracted angle is found for 100 GPa.

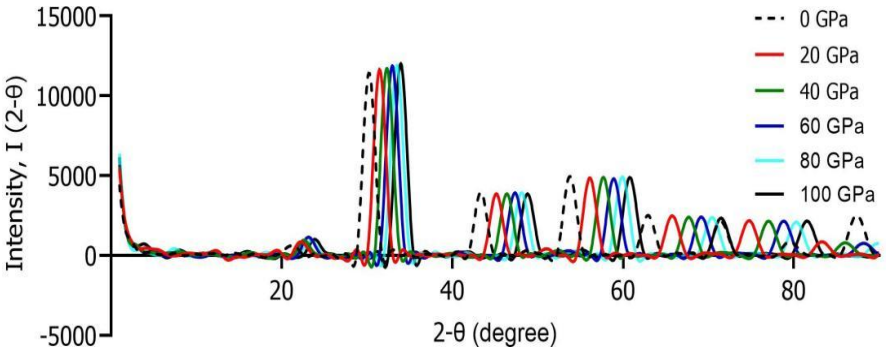

Fig. 9. Evolution of the intensity of diffracted X-rays (colour online)

4. Conclusion

In summary, this research shows that a thorough examination of the density of states, mechanical characteristics, and electronic band structure can yield important information about how different types of materials behave. The density of states showed that specific strontium states cause the conduction band to develop, while specific oxygen states contribute to the upper valance band. The absorption peak shifts toward higher energy according to the optical characteristics, reaching its maximum absorption at about 38.50 eV. The calculations show that the dielectric function has a magnitude of 7, the energy loss function has a magnitude of 8.5 at approximately 33 eV, and the refractive index is 2.7. Thus, these findings contribute to the understanding of $SrSnO_3$ and its potential applications in electro-optic devices, UV filters, photo catalysis, batteries, fuel cells, and high-temperature superconductivity.

Conflicts of interest

The authors have no conflicts of interest to declare.

Data availability

Research data will be made available upon reasonable request.

References

[1] H.-R. Liu, J.-H. Yang, H. J. Xiang, X. G. Gong, S.-Huai. Wei, Applied Physics Letters **102**, 112109 (2013).
[2] H. Shaili, El Mehdi Salmani, Mustapha Beraich, Rida Essajai, Wafaa Battal, Mouad Ouafi, Abderrahim Elhat, Mustapha Rouchdi, M'hamed Taibi, Hamid Ez-Zahraouy, Najem Hassanain, Ahmed Mzerd, Optical Materials **107**, 110136 (2020).
[3] M. M. de M. Bezerra, M. C. Oliveira, W. D. Mesquita, A. B. da Silva Junior, E. Longo, M. F. D. C. Gurgel, Orbital: Electron. J. Chem. **13**(3), 227 (2021).
[4] Arya, Aditya Kumar, Varsha Yadav, Hari Prasad Bhaskar, Sushil Kumar, Satyam Kumar, Upendra Kumar, East European Journal of Physics **2022**(4), 164 (2022).
[5] L. Chantelle, André L. Menezes de Oliveira, André L. Menezes de Oliveira**,** Brendan J. Kennedy, Jefferson Maul, Márcia R. S. da Silva, Thiago M. Duarte, Anderson R. Albuquerque, Julio R. Sambrano, Richard Landers, Máximo Siu-Li, Elson Longo, Iêda M. G. dos Santos, Inorganic Chemistry **59**(11), 7666 (2020).
[6] W. Zhang, J. Tang, J. Ye, Journal of Materials Research **22**(7), 1859 (2007).
[7] H. Chen, N. Umezawa, International Journal of Photoenergy **2014**, 643532 (2014).
[8] K. P. Ong, X. Fan, A. Subedi, M. B. Sullivan, D. J. Singh, APL Materials **3**(6), 062505 (2015).
[9] M. M. de M. Bezerra, M. C. Oliveira, W. D. Mesquita, A. B. da Silva Junior, E. Longo, M. F. D. C. Gurgel, Orbital: The Electronic Journal of Chemistry **13**(3), 227 (2021).
[10] S. J. Clark, Matthew Segall, Chris J. Pickard, Philip James Hasnip, Matt Probert, Keith Refson, Mike C. Payne, Zeitschrift fur Kristallographie **220**, 567 (2005).
[11] M. Shakil, Memoona Kousar, S. S. A. Gillani, M. Rizwan, Hafsa Arshad, M. Rafique, M. Zafar, Indian Journal of Physics **96**(1), 115 (2022).
[12] S. Ahmed, M. Shakil, M. Zafar, I. Zeba, R. Ahmad,

S. S. A. Gillani, Physica B: Condensed Matter **591**, 412240 (2020).
[13] S. M. J. Zaidi, M. I. Khan, S. S. A. Gillani, M. S. U. Sahar, S. Ullah, M. Tanveer, Materials Research Express **9**(12), 125501 (2022).
[14] M. Rizwan, Rabia Bibi, Tariq Mahmood, Imran Aslam, Syed Sajid Ali Gillani, Hai Boa Jin, Chuan Bao Cao, Zahid Usman, Ahmad Maqsood, The European Physical Journal Applied Physics **88**(1), 10501 (2019).
[15] P. Saha, M. K. Datta, O. I. Velikokhatnyi, A. Manivannan, D. Alman, P. N. Kumta, Progress in Materials Science **66**, 1 (2014).
[16] M. I. Khan, S. M. J. Zaidi, M. S. U. Sahar, S. S. A. Gillani, M. A. Qaisrani, M. U. Farooq, Journal of Electronic Materials **52**, 5631 (2023).
[17] I. Zeba, M. Ramzan, Riaz Ahmad, M. Shakil, M. Rizwan, M. Rafique, M. Sarfraz, M. Ajmal, S. S. A. Gillani, Solid State Communications **313**, 113907 (2020).
[18] V. V. Bannikov, I. R. Shein, V. L. Kozhevnikov, A. L. Ivanovskii, Journal of Magnetism and Magnetic Materials **320**(6), 936 (2008).
[19] L. Weston, L. Bjaalie, K. Krishnaswamy, C. G. Van De Walle, Physical Review B **97**, 054112 (2018).
[20] A. Vegas, M. Vallet-Regí, J. M. González-Calbet, M. A. Alario-Franco, Acta Crystallographica Section B **42**, 167 (1986).
[21] Q. Liu, J. Dai, X. Zhang, G. Zhu, Z. Liu, G. Ding, Thin Solid Films **519**(18), 6059 (2011).
[22] M. Shakil, A. Akram, I. Zeba, R. Ahmad, S. S. A. Gillani, M. A. Gadhi, Materials Research Express **7**(2), 025513 (2020).
[23] M. Shakil, Sharjeel Hassan, Hafsa Arshad, M. Rizwan, S. S. A. Gillani, M. Rafique, M. Zafar, Shabbir Ahmed, Physica B: Condensed Matter **575**, 411677 (2019).
[24] S. M. J. Zaidi, M. Ijaz Khan, S. S. A. Gillani, M. Sana Ullah Sahar, Sana Ullah, Muhammad Tanveer, Materials Research Express **9**(12), 125501 (2022).
[25] N. Erum, J. Ahmad, Archives of Advanced Engineering Science **2**(1), 24 (2024).
[26] M. I. Khan, S. M. J. Zaidi, M. S. U. Sahar, S. S. A. Gillani, M. A. Qaisrani, M. U. Farooq, Journal of Electronic Materials **52**(8), 5631 (2023).
[27] A. Ghosh, F. Ahmed, Md. J. Ferdous, Mst. M. J. Juhi, M. F. I. Buian, A. A. Miazee, M. Sajid, Md. Maniruzzaman, A. M. Tighezza, Md. F. Ahmmed, Md. S. Islam, Journal of Physics and Chemistry of Solids **191**, 112053 (2024).
[28] M. Riaz, M. S. U. Sahar, S. M. Ali, M. F. Shah, S. M. J. Zaidi, M. I. Khan, Computational Condensed Matter **37**, e00846 (2023).
[29] M. Riaz, Bakhat Ali, Syed Mansoor Ali, M. Ijaz Khan, M. Sana Ullah Sahar, Mubeen Shahid, Manawwer Alam, Journal of Computational Electronics **23**(3), 483 (2024).
[30] S. M. Junaid Zaidi, M. Sana Ullah Sahar, S. Mansoor Ali, M. Ijaz Khan, M. Faizan Shah, M. Hashim, Results in Optics **13**, 100519 (2023).
[31] X. Luan, H. Qin, F. Liu, Z. Dai, Y. Yi, Q. Li, Crystals **8**(8), 307 (2018).
[32] M. Awais, I. Zeba, S. S. A. Gillani, M. Shakil, M. Rizwan, Journal of Physics and Chemistry of Solids **169**, 110878 (2022).
[33] A. N. Norris, Proceedings of the Royal Society A: Mathematical, Physical and Engineering Sciences **462**(2075), 3385 (2006).
[34] M. A. Ali, R. Ullah, S. A. Dar, G. Murtaza, A. Khan, A. Mahmood, Physica Scripta **95**(7), 075705 (2020).
[35] A. Abdullah, S. M. J. Zaidi, M. I. Khan, M. S. U. Sahar, A. S. Saleemi, Computational Condensed Matter **35**, e00804 (2023).
[36] M. H. Miah, Noor-E. Ashrafi, Md. Bulu Rahman, Mohammad Nur-E-Alam, Mohammad Aminul Islam, K. A. Naseer, Mohamed Y. Hanfi, Hamid Osman, Mayeen Uddin Khandaker, Materials Chemistry and Physics **319**, 129377 (2024).
[37] F. T. Zahra, M. M. Islam, M. M. Hasan, M. R. Islam, S. Ahmad, Journal of Physics and Chemistry of Solids **191**, 112037 (2024).
[38] G. Ajay, M. M. S. Sirajuddeen, V. Ashwin, Chemical Physics Impact **8**, 100431 (2024).
[39] M. Riaz, S. D. Ali, M. Sadiq, M. Ali, S. M. Ali, Chemical Physics **577**, 112141 (2024).

*Corresponding author: ijazkhan4123@gmail.com